American Journal of Biomedical Science & Research

www.biomedgrid.com

ISSN: 2642-1747

Research Article

Wuzi Yanzong Prescription Relieves FSGS by Regulating MSC-Related Hub Genes

Yuanyuan Li[a,b,*], Rongshan Li[a,c*]

[a]*Fifth Clinical Medical College of Shanxi Medical University, China*

[b]*Postdoctoral workstation, Shanxi Provincial People Hospital, China*

[c]*Shanxi Kidney Disease Institute, China*

***Corresponding author:** Yuanyuan Li and Rongshan Li, Fifth Clinical Medical College of Shanxi Medical University, China, Postdoctoral workstation, Shanxi Provincial People Hospital, China, Shanxi Kidney Disease Institute, China.

To Cite This article: *Yuanyuan Li*, Rongshan Li*, Wuzi Yanzong Prescription Relieves FSGS by Regulating MSC-Related Hub Genes. Am J Biomed Sci & Res. 2026 31(4) AJBSR.MS.ID.004055,* **DOI:** 10.34297/AJBSR.2026.31.004055

Received: June 15, 2026 **Published:** 23-06-2026

Abstract

Focal Segmental Glomerulosclerosis (FSGS) is an important cause of end-stage renal disease. Renal resident Mesenchymal Stem Cells (MSCs) play a dual role in FSGS: tissue repair and fibrosis promotion. Currently, drug resistance to steroids and inhibitors is a major challenge for many FSGS patients. However, the application of Chinese medicine, such as Wuzi Yanzong Prescription (WYP), with an active role in the treatment of kidney deficiency, has attracted researchers' attention. In this study, the hub genes related to MSCs and FSGS combined with the active ingredients of WYP were identified by network pharmacological analysis. The top ten proteins related to hub genes were selected, among which three active ingredients (quercetin, matrine, and dinatin) were successfully docked into the binding pockets of four proteins (IL6, MYC, STAT3 and PTGS) with low binding energy according to molecular docking analysis. In a cell-based assay, cotreatment with MSCs and WYP rescued HK-2 cells from injury caused by doxorubicin, with reduced Reactive Oxygen Species (ROS) levels and less DNA damage. Afterwards, we verified the expression levels of the top ten target genes and the effects of WYP treatment in animal experiments. The results revealed that symptoms in the FSGS rat model markedly improved, with significant decreases in urea, creatine, triglyceride, and low-density lipoprotein levels and an increase in phosphorus levels. Specifically, compared with those in untreated FSGS rats, the podocyte ultrastructure clearly improved, and the number of foot processes increased in the kidneys of rats treated with WYP. Additionally, at the molecular level, the expression levels of the top ten genes greatly differed between the model rats and WYP-treated rats; for example, the expression of IL6 and MYC tended to decrease, although the difference was not statistically significant. In contrast, STAT3 expression was significantly greater in the FSGS group than in the normal group, and this increase was significantly lower in the WYP group. Similar increases in the expression of the PTGS2, CCNA2, NFKBIA and STAT1 genes were observed in the FSGS group, and these were decreased after WYP treatment. CAV1 and SERPINEL had similar trends but were not significantly different. The CCND1 expression in the WYP treatment group decreased dramatically, but it significantly increased in the FSGS group. These findings demonstrate that WYP potentially affects FSGS by regulating the expression of key genes related to MSCs and other renal cells. This study provides new perspectives on the molecular mechanism of WYP and provides a basis for WYP in MSCs and renal damage, which will provide a new direction for FSGS treatment.

Introduction

Focal Segmental Glomerulosclerosis (FSGS) is a pathological pattern characterized clinically by proteinuria, hypoproteinaemia and progressive renal function decline. In recent years, the incidence of FSGS has been increasing worldwide [1]. An epidemiological investigation in the United States revealed that the standardized prevalence rate of FSGS was 212.6 cases per million population [2], with a rising trend during the investigation period, especially among black and Asian populations with primary FSGS [3]. The prognosis of patients with FSGS is extremely poor, with three-fourths of these patients progressing to End-Stage Renal Disease (ESRD) at follow-up visits [4]. Currently, the therapeutic options for FSGS are limited to mainly corticosteroids and immunosuppressants, and even after kidney transplantation, the recurrence rate is 20 to 40% [5]. The kidney is a complex tissue composed of more than thirty types of intrinsic cells, among which mesenchymal cells are

distributed mainly in the glomeruli and perivascular spaces of the cortex and renal capsule [6-8]. Renal-intrinsic Mesenchymal Stem Cells (MSCs), especially those derived from pericytes, play "double-edged sword" roles. Under physiological conditions, pericytes can develop into MSCs, which have potential therapeutic ability to protect blood vessels and maintain microenvironmental stabilization [9,10]. When acute injury occurs in the kidney, they can improve tissue regeneration and regulate immunity through paracrine signalling [11-14]. However, in chronic kidney disease, these cells can transdifferentiate into myofibroblasts to induce scar formation [15]. It has rarely been reported that medicine affects renal intrinsic MSCs.

Wuzi Yanzong Prescription (WYP) is a famous classical formula composed of Semen Cuscutate (Tusizi), Fructus Lycii (Gouqizi), Fuructus Rubi (Fupenzi), Fructus Schisandrae (Wuweizi) and Plantaginis (Cheqianzi). Since the Tang Dynasty, ancient Chinese doctors have treated patients with infertility induced by kidney depletion [16]. Modern clinical studies have demonstrated that the application scope of WYP has expanded to include chronic kidney diseases, chronic nephritis, nervous system protection in Parkinson's disease and other diseases [16-18]. On the basis of Chinese medical theory, WYP can be used to treat these diseases by tonifying the kidneys and liver. FSGS is characterized by root deficiency and secondary excess. Here, root deficiency primarily involves kidney deficiency, and the secondary excess is related to pathological characteristics, which are similar to those of Zheng Ji. Zheng Ji is caused by stagnation, usually a combination of blood stasis, phlegm or food retention, and is a type of kidney collateral disorder [19,20]. Given the unsatisfactory outcomes of resistance to corticosteroids and immunosuppressants in FSGS treatment, WYP represents a promising therapeutic approach.

In this study, we constructed an FSGS rat model, treated the rats with WYP, and explored whether WYP affects FSGS and whether its effects are related to intrinsic MSCs. To this end, we conducted network pharmacology and bioinformatics analyses of WYP and MSCs, serological analysis, pathological analysis and bulk RNA sequencing. Through these experiments, we revealed that WYP can alleviate the symptoms of FSGS and influence the expression levels of genes associated with MSCs.

Materials and methods

Network pharmacology and molecular docking analyses

The active ingredients of WYP were screened based on oral bioavailability≥30% and drug-like properties ≥0.18 in the Traditional Chinese Medicine Systems Pharmacology Database and Analysis Platform (TCMSP, https://www.tcmsp-e.com/), and the gene targets of the active ingredients were obtained through the Swiss Target Prediction database (http://www.swisstargetprediction.ch/). Disease gene targets were obtained from the Home–OMIM database (https://www.omim.org/) and the GeneCards - Human Genes database (https://www.genecards.org/) using the keyword focal segmental glomerulosclerosis. The genes associated with renal MSCs were obtained from GSE101973 using limma in the SangerBox platform (http://vip.sangerbox.com/), which was screened based on the criteria of P<0.05 and |logFC|≥1. The intersection of the component targets of WYP, the disease targets of FSGS and renal MSC genes was drawn using a Venn diagram (http://bioinformatics.psb.ugent.be/webtools/Venn/). The potential intersection targets were uploaded to the STRING database (https://string-db.org/) for protein-protein interaction (PPI) network analysis, which was visualized using Cytoscape software 3.9.0. The DAVID database (https://david.ncifcrf.gov) was used to analyse the intersection targets to determine Gene Ontology (GO) and Kyoto Encyclopedia of Genes and Genomes (KEGG) pathway enrichment.

The crystal structures of the top five core ingredients were obtained from UniProt (https://www.uniprot.org/), and the CDOCKER energy and CDCKER interaction energy were calculated by Discovery Studio software. With the standard of interaction ≤-5.0 kcal/mol, the core target protein with the corresponding compound was imported into the DS BIOVIA Discovery Studio 2016 for molecular docking and visualization using PyMOL software.

Effects of WYP on cells

Cells Preparation: HK-2 (human kidney proximal tubule) cells were purchased from Procell Life Science & Technology Co., Ltd. (Wuhan, China). Human umbilical cord-derived MSCs were purchased from Shanxi Cell Therapy Technology Group Co., Ltd. (Taiyuan, China). HK-2 cells and MSCs were cultured in complete medium composed of DMEM/F12 supplemented with 5% Foetal Bovine Serum (FBS), 1% penicillin/streptomycin, and 1 ng/mL basic Fibroblast Growth Factor (bFGF), with a seeding density of 1.0*104 on cell culture plates in an incubator at 37°C and 5% CO2. When the cellular confluence reached 90%, the cells were digested with 0.25% trypsin-ethylenediaminetetraacetic acid (EDTA), and the digestion reaction was terminated with complete medium.

CCK-8: HK-2 cells were collected, counted, resuspended, inoculated into 96-well plates and incubated in an incubator. At the logarithmic growth period and at 80% confluence, the control wells were supplemented with 100μL of fresh complete culture medium, and the other wells received 8μM doxorubicin (Hydroxydaunorubicin, MedChemExpress LLC). Twenty-four hours later, all the medium was aspirated. The control and model wells were replenished with 100 μL of fresh medium, and the remaining wells were separately treated with different concentrations of WYP (40, 80, 100, 150, or 200μg/mL). After 24 h, CCK-8 reagent was added to all the wells, and the absorbance was measured using an ELISA reader after 1 h of incubation.

Reactive Oxygen Species Assay: All the cells were resuspended and cultured in coculture plates. HK-2 cells were plated on 24-well plates, and MSCs were plated in chambers with 0.4 μm pores suitable for 24-well plates. After 2 days, when the HK-2 cells had reached 80% confluence, they divided into five groups: control, model, MSC treatment, MSC&WYP treatment and WYP treatment. The medium was removed, and new medium supplemented with 8μM doxorubicin was added to all the groups except the control group. Twenty-four hours later, the medium in all the groups was changed, the chambers with MSCs were placed into wells for the

MSC treatment and MSC&WYP treatment, and WYP was added at a concentration of 150μg/mL. After another 24h, in accordance with the instructions of the reactive oxygen species assay kit (Beyotime, China), all the wells were rinsed with extracellular solution twice, and DCFH-DA (diluted 1:1000 with extracellular solution) was added; the samples were incubated in an incubator for 2 h and then subjected to high-content analysis (Opera Phenix, PerkinElmer, USA).

DNA Damage Test: The cells were cocultured on plates as described above. After the reaction with doxorubicin and treatment with MSCs and WYP as described for the ROS assay methods, the wells were stained with a DNA damage detection kit (Beyotime, China) according to the instructions. After they were rinsed and blocked, the primary antibody anti-γ-H2AX (rabbit-derived monoclonal antibody) and the secondary anti-rabbit antibody were reacted, after which the high-content analysis was performed.

Statistical Analysis: The images of the ROS and DNA damage tests were analysed using ImageJ software to measure the grey levels. One-way analysis of variance (ANOVA) with multiple comparisons in GraphPad Prism 10.3.0 (GraphPad Software Inc., San Diego, CA, USA) was used to evaluate the differences among the groups. The results are presented as the means±SDs. $P<0.05$ was considered to indicate statistical significance.

Animal Experiments

Model Animal Construction: Fifteen 6-week-old Sprague-Dawley (SD) rats were purchased from SPF Biotechnology Co., Ltd. (Beijing). The rats were housed in the Animal Laboratory Facility under a free access environment with water and food available ad libitum. The housing conditions included a constant temperature of 25±2°C, 40%-70% humidity and a 12 h light/12 h dark cycle. All experimental procedures were performed in strict accordance with the Principles of Laboratory Animal Care and were approved by the Ethics Committee of Shanxi Provincial People's Hospital (Ethics approval No. 353). After one week of acclimatization, all the rats were randomly assigned to one of three experimental groups (n=5 rats per group): control, FSGS and WYP treatment. The rats in the FSGS and WYP groups underwent left nephrectomy under continuous inhalation of 2% isoflurane in oxygen (v/v) administered through a rodent anaesthesia vaporiser (Shanghai Yuyan Instruments Co., Ltd.). The rats in the control group underwent a sham operation, in which a skin incision was made over the kidney to expose the kidney for several minutes, matching the same amount of time as that in the other groups, without undergoing nephrectomy. All surgeries were performed according to standard aspiration techniques. After surgery, the rats were injected with 0.4mg/kg meloxicam (Jiangsu Feima Pharmaceutical Co., Ltd., H20030392) once daily for 3 days for postoperative nephrectomy analgesia. To avoid infection, benzylpenicillin sodium (CSPC Pharmaceutical Group Ltd., H51021742) was administered intramuscularly at a dosage of 100,000 IU/day for 3 consecutive days. The rats in both the FSGS and WYP treatment groups received a single intravenous injection of 4mg/kg doxorubicin via the tail vein on day 7 after surgery, followed by a second dose of 2mg/kg doxorubicin on day 28 [21]. Moreover, the rats in the control group received an equivalent volume of saline via the same route. From the first day after the second doxorubicin treatment, the rats in the WYP group were administered 1.4g/kg/d via intragastric infusion for 8 weeks, whereas the rats in the control and FSGS groups received an equivalent amount of distilled water daily via intragastric infusion [22].

At 12 weeks post-surgery, all the rats received deep anaesthesia with 4% isoflurane in oxygen (v/v) at a flow rate of 1 L/min. After the rats completely lost their sense of pain, as indicated by dilated pupils and no response to painful stimuli, blood was collected via cardiac puncture. The rats were subsequently euthanized with 5% isoflurane for 10 minutes, after which the kidneys of all the rats were immediately harvested. All the kidneys were divided into three parts: one was fixed with 4% paraformaldehyde, embedded in paraffin, and sectioned at 2μm for histological staining; approximately 1 mm3 of tissue cut from another part was fixed in 2.5% glutaraldehyde and stored at 4°C for Transmission Electron Microscopy (TEM); and the other part was used for RNA sequencing. Blood was centrifuged at 3000*g for 10minutes at room temperature. After separation and aliquoting, the serum was stored at -80°C for further processing.

Histological Staining and Analysis: All kidney sections were deparaffinized in xylene and rehydrated using a graded ethanol series from 100%, 95%, 80, and 70% to triple-distilled water. The sections were stained with haematoxylin and eosin (HE), Periodic Acid-Schiff (PAS), and Masson's trichrome according to the instructions of the respective kits (G1120, G1281, and G1340; Solarbio Life Sciences, China). Afterwards all the sections were dehydrated through a graded series of 70%, 80%, 90% and 100% ethanol; cleared in xylene; and mounted with neutral balsam. Images were captured with a disgital pathological section scanner (KF-PRO-005-EX, KONFOONG BIOINFORMATION TECH, China).

TEM: The fixed tissue was rinsed three times for 15minutes each with PBS and incubated with 1% osmium tetroxide (OsO_4) at 4°C overnight in the dark. The tissue was dehydrated through a graded ethanol series, soaked in pure acetone/propylene oxide for 10minutes twice, embedded in Epon 812, sectioned with a fine blade, subjected to thin sectioning, and underwent toluidine blue staining, after which the observation area was located under optical microscopy. The sections were cut to 60nm by an ultrathin sectioning machine, loaded onto 300-mesh copper slides, stained with uranium acetate, treated with lead citrate and captured under a Hitachi HT7800 TEM at 80-120 kV.

Serum Biochemical Assay: Serum levels of urea, Creatinine (crea), Triglyceride (TG), total Cholesterol (CHOL), High-Density Lipoprotein Cholesterol (HDL-C), Low-Density Lipoprotein (LDL), Phosphorus (P), Total Protein (TP), Albumin (ALB), and Calcium (Ca) were measured by the Beijing North Institute of Biotechnology Co., Ltd. All the results were analysed using GraphPad Prism 10.3.0 (GraphPad Software Inc., San Diego, CA, USA).

Transcriptome: The kidney tissues from the abovementioned rats were immediately snap-frozen in liquid nitrogen and stored at

-80°C until RNA sequencing. The tissues were delivered to Sangon Biotech (Shanghai) Co., Ltd., to extract total RNA, construct a library, and conduct sequencing on an Illumina platform for bioinformatics analysis.

Statistical Analysis

All the data are presented as the means ± Standard Deviations (SDs) of at least three independent experiments. One-way ANOVA with multiple comparisons was used to compare groups using GraphPad Prism 10.3.0 (GraphPad Software Inc., San Diego, CA, USA), and *p<0.05 was considered to indicate a statistically significant difference.

Results

Network pharmacology and the PPI network

In the TCMP database, the active ingredients of the five herbs composing WYP had 191 targets, which were subsequently transformed into gene names using the UniProt database. The components of quercetin, matrine, dinatin (hispidulin), dihydrotricetin, and hypolaetin had the greatest degree of freedom, demonstrating that they may be the key active components and have the greatest binding energy with the targets. These target genes, the genes associated with FSGS and the genes associated with renal MSCs were crossed, resulting in the formation of a drug–component–target network (Figure 1A). The intersection revealed 27 genes. On the basis of the PPI network with 27 nodes and 125 edges, the top ten targets, namely, IL6, MYC, STAT3, PTGS2, CCND1, CCNA2, CAV1, NFKBIA, SERPINE1, and STAT1, were predicted to be targets of WYP, potentially regulating renal intrinsic MSCs and the treatment of FSGS (Figure 1B). Gene Ontology enrichment analysis for the targets of WYP was conducted for three functional categories, namely, Cellular Component (CC), Biological Process (BP) and Molecular Function (MF). In the BP domain, oxygen levels, the response to hypoxia, and cytokine-mediated signalling were significant. The CC domain was significantly enriched in the cyclin-dependent protein kinase holoenzyme complex and focal adhesion. In the MF category, DNA-binding transcription factor and cytokine receptor binding were the most enriched terms (Figure 1C). These results showed that WYP may modulate the hypoxia response and cytokine signalling of renal intrinsic MSC and FSGS genes in the treatment of FSGS.

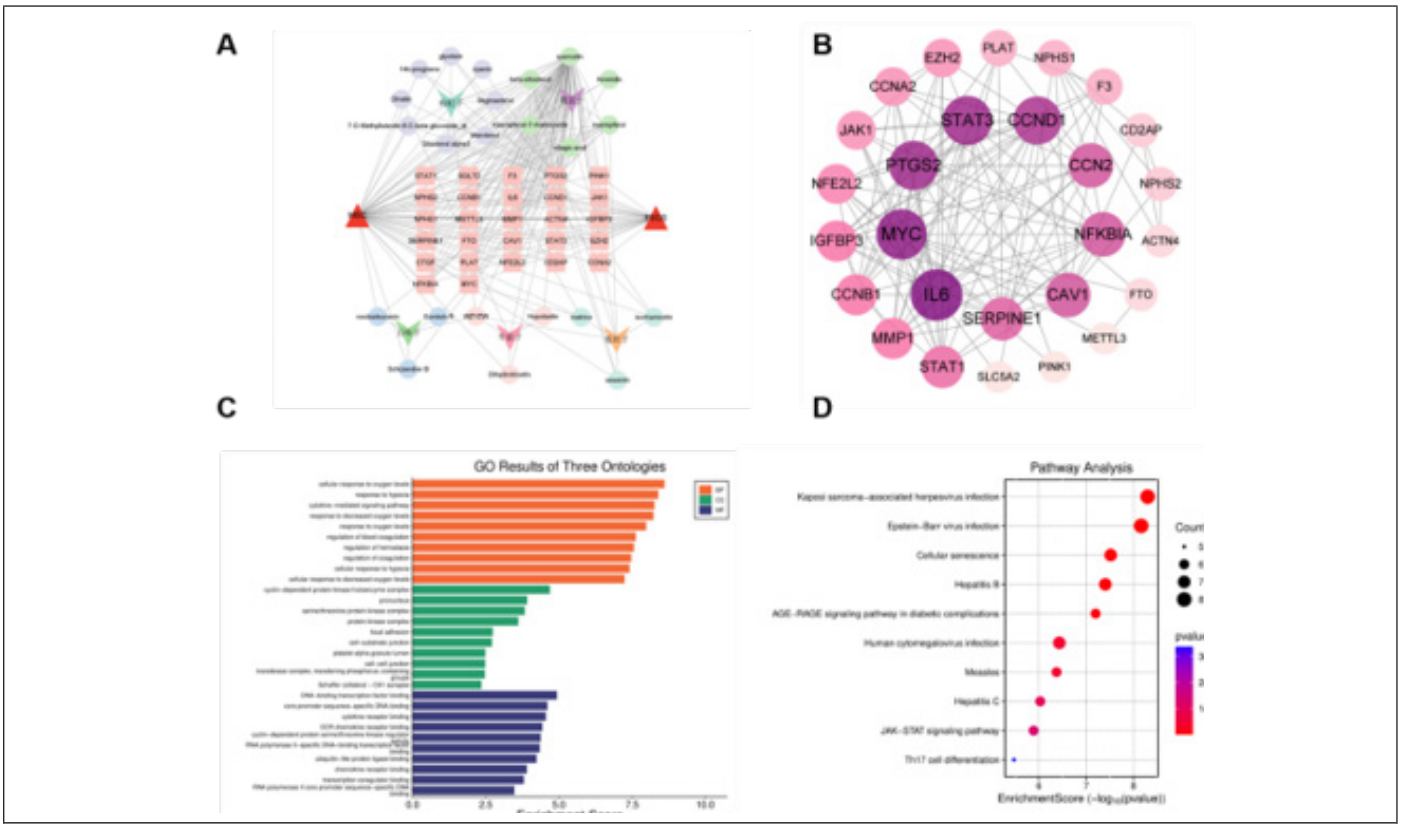

Figure 1: Network and bioinformatic analyses. (A) Network analysis of WYP–active ingredients–intersecting genes–MSCs–FSGS; note that the ovals represent active ingredients, the red triangles represent MSCs and FSGS, and the pink rectangles represent intersecting genes. (B) Protein-protein interactions (PPIs) of 27 genes were constructed using STRING and Cytoscape software with confidence values greater than 0.4; note that the degree of protein association is represented by the thickness of the lines. (C) GO functional enrichment analysis of 27 intersecting genes; the GO terms are sorted according to the P value, and the ordinate shows each GO term; the horizontal coordinate represents the ratio of genes, the number of genes is represented by the length of the column, orange represents BP, green represents CC, and dark blue represents MP. (D) KEGG pathway enrichment analysis. The horizontal coordinate represents the gene proportion, and the vertical coordinate represents the gene pathway term enriched by KEGG. The dot size represents the number of enriched genes, and the colour represents the P value.

The results of the KEGG enrichment analysis of the mechanism underlying WYP regulation of MSCs and treatment of FSGS were related to cellular senescence, the AGE-RAGE signalling pathway in diabetic complications, the JAK-STAT signalling pathway and Th17 cell differentiation (Figure 2D). Among the top ten targets with the greatest degree, the top three proteins were subjected to molecular docking with the active compounds. According to their binding energy, which was ranked from lowest to highest (Table 1), six compound-target pairs were successfully identified (Figure 2).

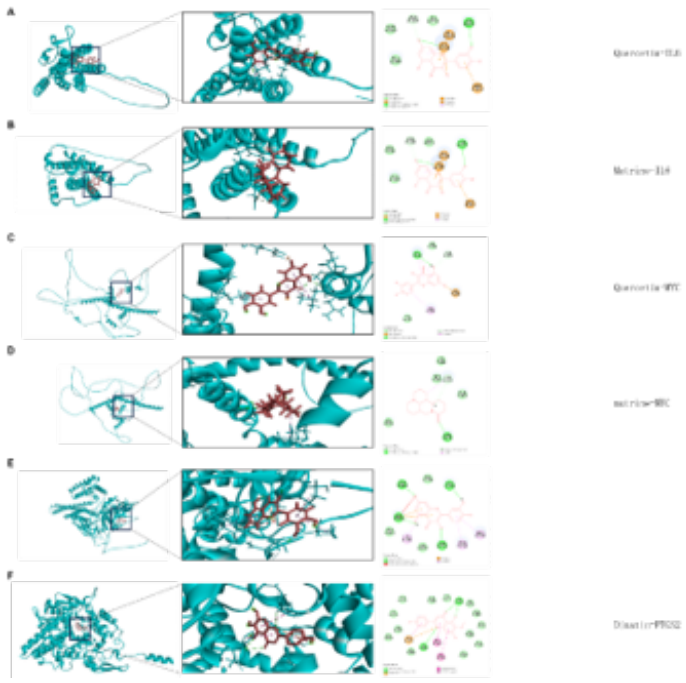

Figure 2: Molecular docking patterns of selected targets and specific active ingredients. (A1) Quercetin-IL6, (B1) matrine-IL6, (C1) quercetin-MYC, (D1) matrine-MYC, (E1) quercetin-STAT3, and (F1) dinatin-PTGS2. (A2), (B2), (C2), (D2), (E2) and (F2) show two-dimensional patterns of bonds during docking.

Table 1: Molecular docking binding energies (kcal/mol).

Active Ingredient	Protein	Cdockep Energy	Cdocker Interaction
Quercetin	IL6	-31.3281	-43.3493
Matrine	IL6	-17.5904	22.4929
Quercetin	MYC	-36.092	-41.2277
Matrine	MYC	-25.3967	-17.4869
Quercetin	STAT3	-31.9885	-39.2795
Dinatin	PTGS2	15.2358	-21.9463
Dihydrotricetin	PTGS2	Not valid	
Hypolaetin	PTGS2	Not valid	
Quercetin	PTGS2	14.8347	-9.2412
Ammidin	PTGS2	Not valid	
Beta-sitosterol	PTGS2	Not valid	
Kaempferol	PTGS2	16.2947	-18.4871
Kaempferol-7-rhamnoside	PTGS2	Not valid	
Sitosterol alpha1	PTGS2	9.56711	-21.3874
Mandenol	PTGS2	-1.2783	-29.4583
Stigmasterol	PTGS2	Not valid	
Cyanin	PTGS2	5.3782	-31.4721
Glycitein	PTGS2	Not valid	

WYP protects HK-2 cells against oxidative stress injury induced by doxorubicin

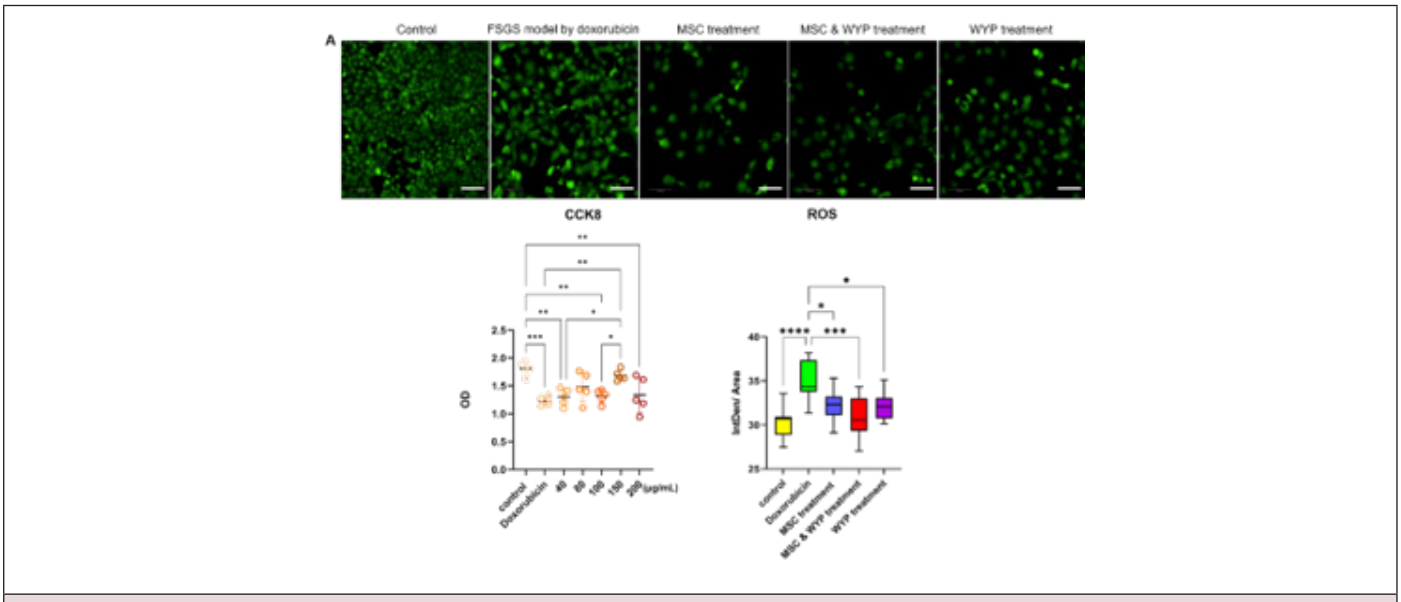

Figure 3: ROS protein expression levels in the HK-2 cells in each group. (A) ROS fluorescence staining; the scale bar is 100μm. (B) CCK-8 assay results showing the effects of different concentrations of WYP on HK-2 cells treated with doxorubicin. (C) Statistical analysis of ROS fluorescence by ImageJ software (*P<0.05, **P<0.01, ***P<0.001, ****P<0.0001).

The results of the CCK-8 assay revealed that 150μg/mL WYP was the optimal concentration for increasing HK-2 cell viability (Figure 3B). On the basis of these results, 150μg/mL WYP was used to rescue the damage to HK-2 cells induced by doxorubicin, and the effects of MSC and WYP treatment on the oxidative stress induced by doxorubicin were assessed by measuring intracellular ROS generation (Figure 3A). ROS production increased in the doxorubicin group; in contrast, treatment with MSCs and WYP effectively attenuated the oxidative stress induced by doxorubicin. Compared with doxorubicin alone, the combination therapy with MSCs and WYP had the greatest antioxidant effect, with a highly significant reduction in ROS levels (P<0.001). Compared with the doxorubicin group, the MSC monotherapy and WYP monotherapy groups demonstrated significant decreases in ROS accumulation (P<0.05) (Figure 3C).

Doxorubicin-induced reactive oxygen species damaged the DNA of HK-2 cells, and treatment with MSCs and WYP alleviated the DNA damage in HK-2 cells. The γ-H2AX fluorescence staining results of the DNA damage test revealed that the densities decreased in the MSC&WYP and WYP groups (Figure 4A). Based on the statistical distribution of the grayscale values obtained by ImageJ, compared with the doxorubicin group, the MSC&WYP therapy group demonstrated a marked reduction in the density; however, the decrease in DNA damage in the MSC group was not statistically significant (Figure 4B).

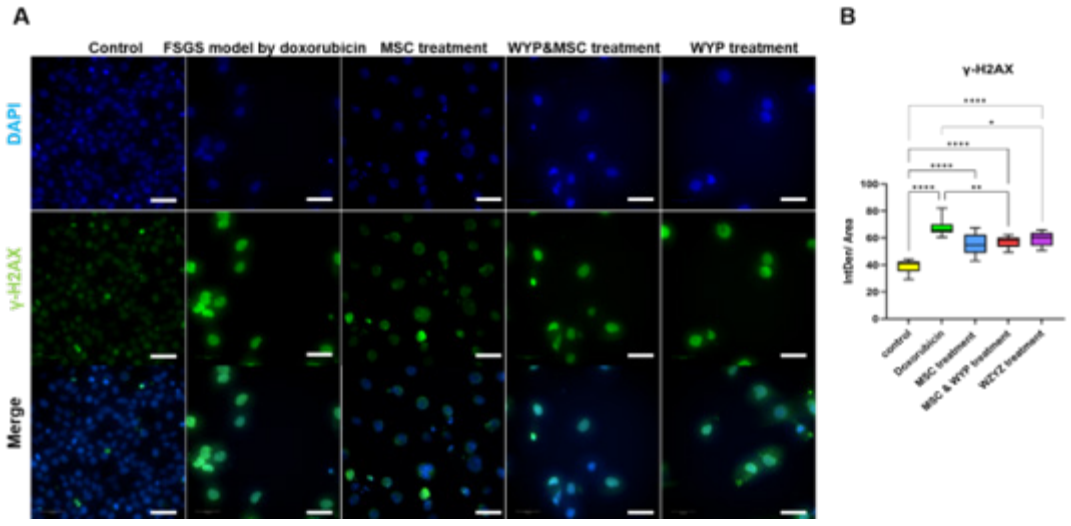

Figure 4: γ-H2AX expression in the HK-2 cells in each group. (A) High-content imaging of γ-H2AX in HK-2 cells injured by doxorubicin and treated with MSC and WYP (scale bar is 50μm). (B) Statistical analysis of γ-H2AX fluorescence by ImageJ software (*P<0.05, **P<0.01, ***P<0.001, ****P<0.0001).

Pathological Analysis

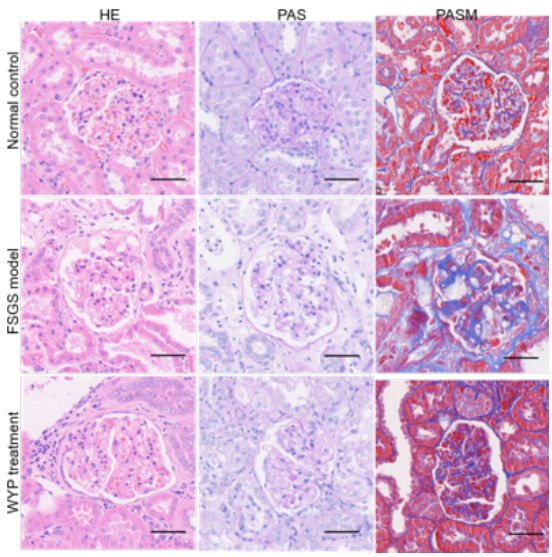

Figure 5: Histological staining results for the three groups. HE and PAS staining revealed that the glomeruli exhibited adhesion of the glomerular capsule (black arrow) and vacuoles (red arrow), and Masson staining revealed staged glomerular sclerosis and tubular fibrosis (blue) in the FSGS group. In the WYP group, these pathological features decreased. The scale bar is 100μm.

Kidney sections from all three groups were subjected to HE, PAS and Masson's trichrome staining. In the normal control group, the glomeruli had patent loops with delicate basement membranes and a normally limited mesangial matrix and cellularity. In the FSGS group, significant mesangial expansion, capsular thickening, synechiae formation, crescent formation, and increased extracellular matrix deposition were confirmed by PAS staining, whereas more collagen accumulated in the glomeruli and tubulointerstitium, as shown by Masson's trichrome staining. In contrast, less extracellular matrix deposition and collagen were detected in the WYP-treated group than in the FSGS model group (Figure 5).

Podocyte Foot Procession Revealed by TEM

Podocyte ultrastructure was evaluated by TEM. In the normal control group, podocyte feet presented as regularly interdigitating Foot Processes (FPs) with intact slit diaphragms along the Glomerular Basement Membrane (GBM) (Figure 6, black arrow). In the FSGS group, the podocytes were injured and exhibited extensive Foot Process Effacement (FPE), with broad, continuous sheets of cytoplasmic flattening instead of finger-like FPs (Figure 6, red arrow). Following WYP treatment, FPE was markedly attenuated, with the restoration of discrete FPs (Figure 6, blue arrow).

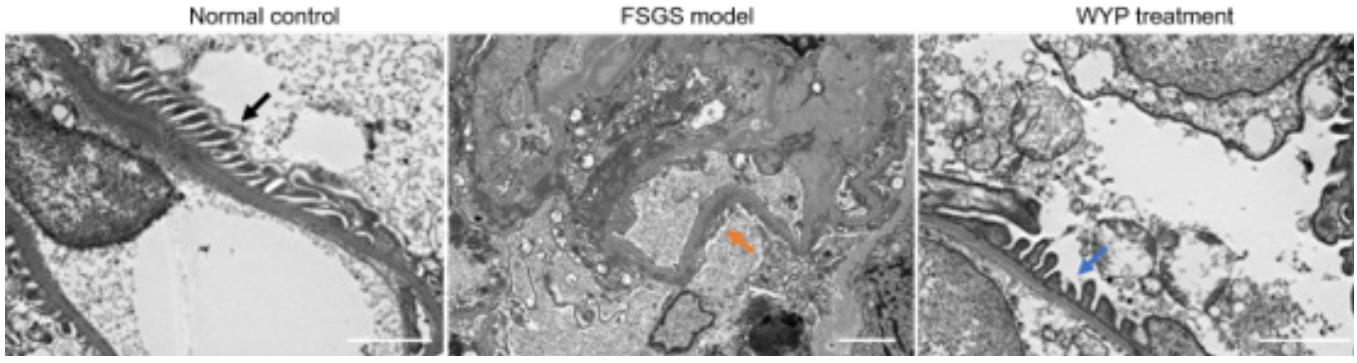

Figure 6: WYP treatment attenuated podocyte foot process effacement in FSGS. Representative Transmission Electron Microscopy (TEM) images of glomerular capillary loops. (A) Normal control showing regularly spaced foot processes (black arrow). (B) FSGS model group showing extensive Foot Process Effacement (FPE), characterized by continuous cytoplasmic spreading along the glomerular basement membrane (GBM; red arrows). (C) WYP treatment group showing significant preservation of podocyte architecture, with distinct, interdigitating foot processes clearly visible (blue arrow). The scale bar is 2μm.

Serum Biochemistry

Detection of serum parameters revealed profound disorders in the metabolic functions of proteins, lipids and minerals in the FSGS model, which were alleviated by WYP. Compared with normal controls, FSGS rats presented apparent renal damage and dramatically elevated serum urea and creatine levels (P<0.001) (Figure 7A–B). WYP administration dramatically decreased both the urea and creatinine levels (P<0.05). With respect to lipid metabolism, compared with those in the normal controls, the serum lipid levels of all four tested lipids in the FSGS model group clearly increased (P<0.01), while the LDL level was greatly increased (P<0.001); by contrast, the TG level and LDL level decreased significantly in the WYP group (P<0.05) (Figure 7C-F). Changes in protein metabolism are induced by kidney injury. ALB levels were significantly lower in the FSGS group than in the normal control group (P<0.001). In the WYP group, the ALB concentration tended to increase, but the difference was not significant (Figure 7H). The TP in the three groups was not different (Figure 7G). Similar to the case of ALB, P was dramatically greater in the FSGS model group than in the normal control group (P<0.01) and was lower in the WYP group (P<0.05) (Figure 7I). Compared with that in the normal control group, the Ca level in the FSGS group was increased, whereas there was a slight downward trend that was not significant in the WYP group (Figure 7J).

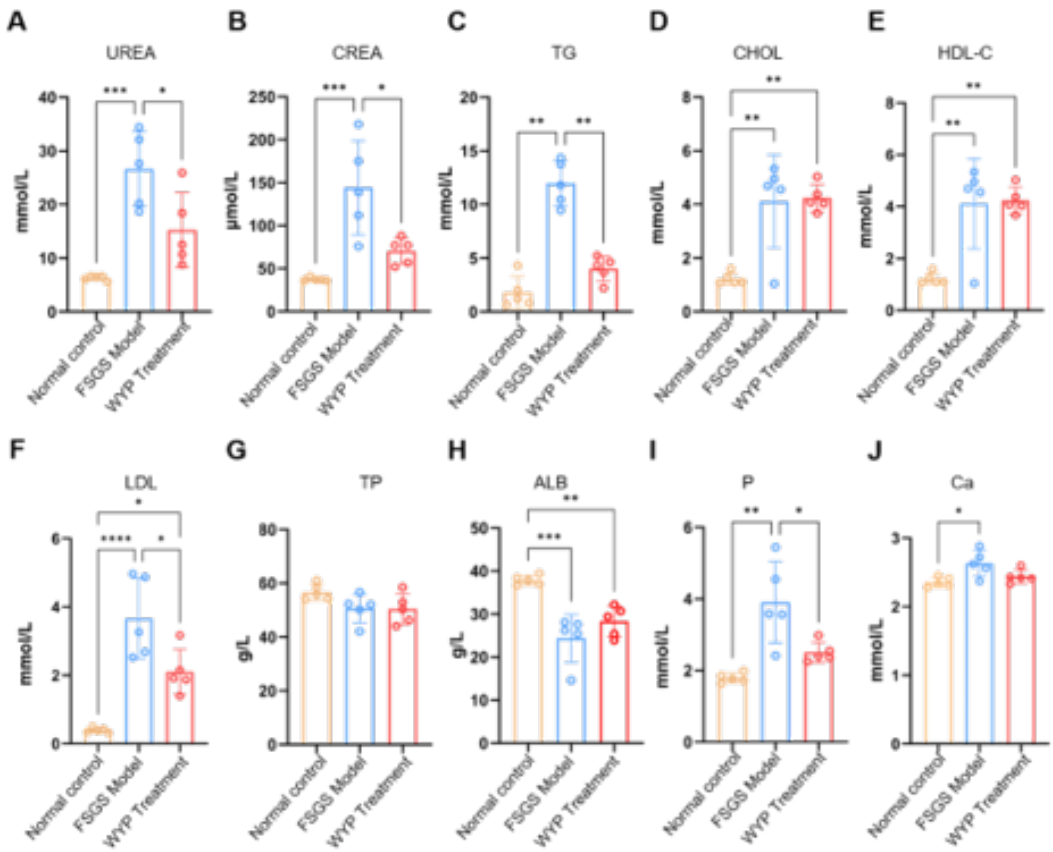

Figure 7: Serum biochemical parameters in the animal experiments. (A-B) Serum urea and creatinine levels. A significant difference was observed between the FSGS and normal groups (P<0.001) and a notable decrease in the WYP group (P<0.05). (C-F) Compared with those in the normal group, the levels of all four serum lipids in the FSGS group were significantly different (P<0.01), especially low-density lipoprotein, which showed the most marked increase (P<0.001). Triglyceride (TG) and LDL levels decreased significantly in the WYP treatment group (P<0.05). (G) The total protein level did not significantly differ across the three groups. (H) Albumin (ALB) levels significantly decreased in the FSGS group compared with those in the normal group (P<0.001), while there was an increasing trend in the WYP group, but the difference was not significant. (I) Compared with that in the normal group, the serum phosphorus (P) level in the FSGS group was elevated (P<0.01); this status was reversed following WYP treatment. (J) Serum calcium (Ca) levels increased in the FSGS group compared with those in the normal group, with a slight nonsignificant downwards trend following WYP treatment. The data are presented as the mean±SD, and statistical analysis was performed with one-way ANOVA (*P<0.05, **P<0.01, ***P<0.001, ****P<0.0001).

Transcriptomic Analysis of Hub Gene Expression Levels

The top ten genes obtained from the network analysis exhibited different transcription statuses. These genes belonged to three functional categories: the inflammatory and immune signalling category of IL6, STAT3, STAT1, NFKBIA, and PTGS2; the cell cycle and proliferation category of MYC, CCND1 and CCNA2; and the fibrosis and matrix remodelling category of CAV1 and SERPINE1. Compared with that in the normal control group, the level of IL6 in the FSGS group was dramatically greater (P<0.001), and it was obviously lower but not significantly different in the WYP treatment group (Figure 8A). MYC expression tended to increase from the normal group to the FSGS group and then to the WYP treatment group, but the difference was not significant (Figure 8B). Among the three groups, STAT3 expression significantly increased in the FSGS group compared with that in the normal group (P<0.05) and in the WYP group (P<0.001) (Figure 8C). PTGS2, CCNA2, NFKBIA and STAT1 levels dramatically increased in the FSGS group compared with those in the normal group (P<0.01) and decreased in the WYP group (P<0.05) (Figure 8D, F, H), whereas CAV1 and SERPINEL did not significantly differ. Additionally, the expression of CCND1 tended to increase sharply in the FSGS group (P<0.001) but obviously decreased in the WYP group (P<0.01).

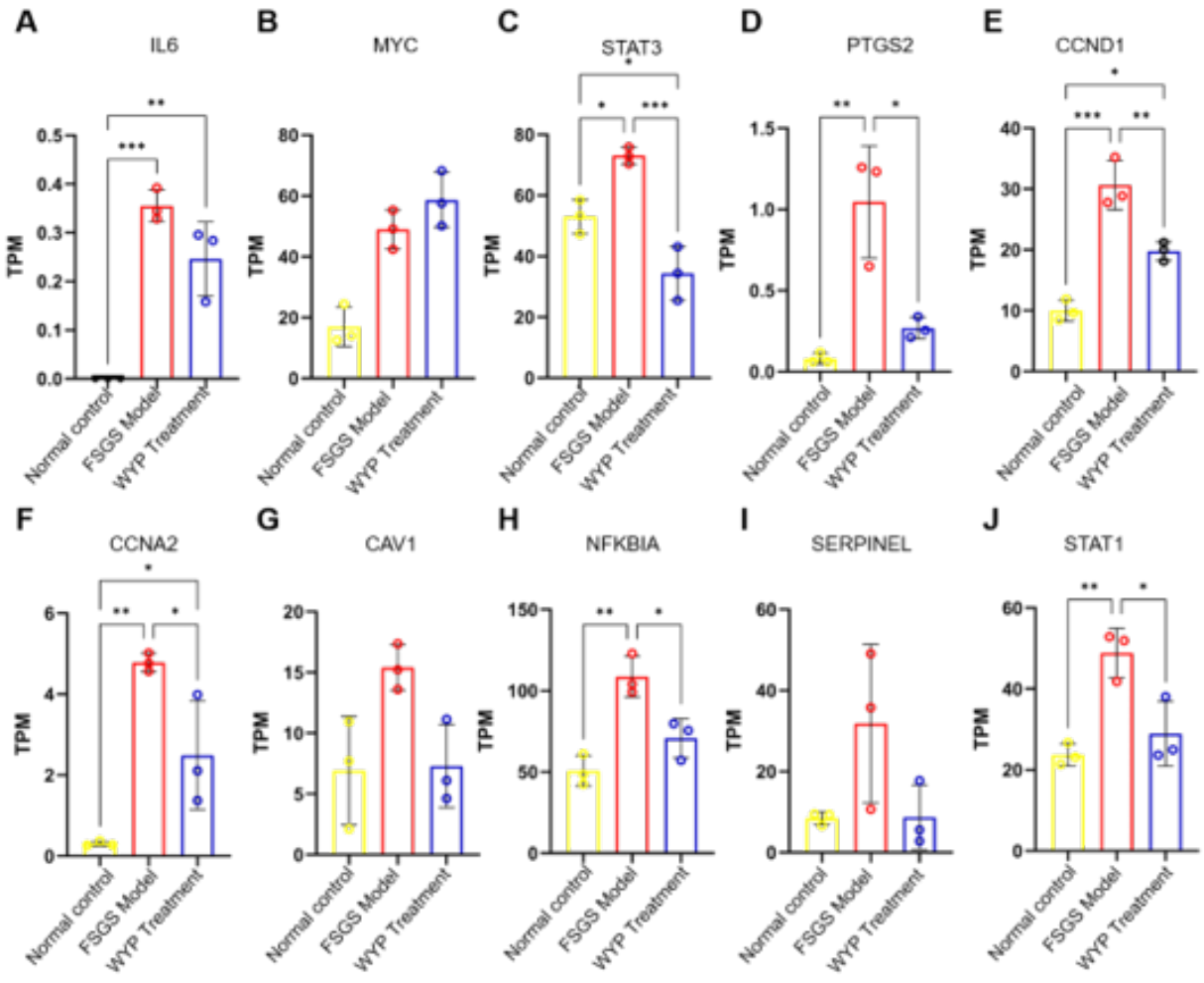

Figure 8: Transcriptional changes in the top ten genes derived from network analysis in animal experiments. (A) IL6 expression was dramatically upregulated in the FSGS group compared with that in the normal group (P<0.001). WYP treatment tended to decrease the expression, but the difference was not significant. (B) MYC expression tended to increase across the three groups, but the difference was not significant. (C) Compared with that in the normal group, STAT3 expression increased in the FSGS group (P<0.05) and was markedly decreased in the WYP group compared with the FSGS group (P<0.001). (D, F, H) The expression levels of PTGS2, CCNA2, NFKBIA and STAT1 increased markedly in the FSGS group (P<0.001) compared with those in the normal group and clearly decreased in the WYP group (P<0.05) compared with the FSGS group. (E, G) CAV1 and SERPINE1 expression tended to increase in the FSGS group compared with that in the normal group but decreased in the WYP group compared with the FSGS group; however, the difference was not significant. (I) CCND1 expression was significantly higher in the FSGS group (P<0.001) than in the normal group and significantly lower in the WYP group than in the FSGS group.

Discussion

FSGS leads to glomerular sclerosis and renal tubular and interstitial fibrosis, ultimately leading to end-stage renal disease, which can be prevented by active intervention measures. On the basis of traditional Chinese medical theory, FSGS derives from kidney deficiency, which is the core of WYP treatment [16]. In this study, we revealed that 27 genes were enriched in processes including hypoxia and oxidative stress and signalling pathways closely related to senescence, proliferation, differentiation and inflammation. The top ten genes expressed in both the MSC and FSGS groups, whose response proteins had strong binding energy and were strongly bound with the active ingredients, were identified. Compared with MSCs or WYP alone, WYP plus MSCs better reduced ROS and DNA damage. Moreover, the results of the rat experiments revealed that WYP alleviated the symptoms of FSGS, improved renal function by decreasing the levels of urea and creatinine, improved lipid metabolic function with lower TG and LDL levels, and improved mineral metabolic function with reduced phosphorus levels. Pathological images demonstrated mitigated glomerular fibrosis and protection of podocyte foot processes.

WYP alleviates renal damage in FSGS through mechanisms related to immune reactions, metabolism, and cell survival. The results of this study revealed that the active ingredients in WYP of quercetin, matrine, dinatin (hispidulin), dihydrotricetin, and hypolaetin obtained by network pharmacology play crucial roles in treatment of FSGS. Quercetin can eliminate senescent cells [23,24] as a senolytic drug and has antioxidant and renoprotective effects [25]; matrine has antioxidative, anti-inflammatory and anti-apoptotic effects [26-28]; and hispidulin decreases autophagy and suppresses apoptosis to protect podocytes [29]. Hypolaetin possesses anti-inflammatory and antioxidant activities [30]. According to the results of molecular docking, IL6 strongly bound to quercetin and matrine, which demonstrated the role of anti-inflammation; MYC had strong binding energy with quercetin and matrine, which revealed the role of proliferation and differentiation; and PTGS2 strongly bound to dinatin, which represented the role of anti-inflammation. These target genes are expressed in renal cells, including MSCs, podocytes, and renal tubular epithelial cells. When they are damaged, the active ingredients of WYP act on them, resisting inflammation (e.g., IL6), inhibiting oxidative damage (e.g., PTGS2) and promoting cell proliferation (e.g., MYC).

MSCs derived from the bone marrow, human umbilical cord and adipose tissue can self-renew, immunoregulate, and undergo multilineage differentiation and cell crosstalk [31-33]. Because of these functions, MSCs have been used to treat FSGS [34-36]. Some Chinese herbs can not only act directly on FSGS but also enhance the function of MSCs, thereby reinforcing damage repair and inhibiting the progression of FSGS [37,38]. However, the intrinsic MSCs represent a double-edged sword. On the one hand, they can assist in repairing damage; on the other hand, they can transform into myofibroblasts, leading to fibrosis [39]. In this study, we determined that WYP can act on genes common to both MSCs and FSGS to alleviate the symptoms of FSGS. This study has several limitations; owing to the limited conditions, we have not verified the specific details of the intrinsic MSCs induced by WYP. In the future, we will perform cell tracing experiments of MSCs and single-cell sequencing experiments to confirm the mechanisms underlying how WYP acts on renal MSCs to affect FSGS.

Conclusion

In summary, we identified hub genes associated with FSGS and MSCs, and WYP alleviated the effects of FSGS on metabolism and cell microstructure, which demonstrated that WYP plays important roles in FSGS treatment. In the future, we will explore the special cell crosstalk between MSCs and other kidney cells by cell tracing and single-cell RNA sequencing to establish a solid basis for WYP clinical treatment.

Acknowledgements

None.

Conflict of Interest

None.

References

1. C Orizaga-de-la-Cruz, FA Lagunas-Rangel, A Gómez-García, V Chávez-Valencia (2025) An approximation to the prevalence of focal segmental glomerulosclerosis: A systematic review of world literature over the past 32 years. Nefrologia 45(10): 501404.
2. ME Bensink, KM Thakker, EV Lerma, RM Lieblich, CM Bunke, et al. (2025) Prevalence, resource utilization, and economic impact of kidney function and proteinuria in patients with focal segmental glomerulosclerosis. The American journal of managed care 32(7).
3. MA Munis, Q Chen, TM Hill, M Zhuo, AD Schachter, SK, et al. (2024) Incidence and Proportion of Primary Focal Segmental Glomerulosclerosis (FSGS) among a Racially and Ethnically Diverse Adult Patient Population between 2010 and 2021 Clinical journal of the American Society of Nephrology: CJASN 20 (22): 229-238.
4. D Goldschmidt, ME Bensink, ZY Zhou, S Shi, Y Lin, et al. (2024) Epidemiology and burden of focal segmental glomerulosclerosis among United States Veterans: An analysis of Veteran's Affairs data, PloS one 19 (12): e0315302.
5. A Uffing, MJ Pérez-Sáez, M Mazzali, RC Manfro, AC Bauer, et al. (2020) Recurrence of FSGS after Kidney Transplantation in Adults. Clinical journal of the American Society of Nephrology: CJASN 15 (2): 247-256.
6. IG Gomez, JS Duffield (2014) The FOXD1 lineage of kidney perivascular cells and myofibroblasts: functions and responses to injury. Kidney international supplements 4 (1): 26-33.
7. HC Park, K Yasuda, MC Kuo, J Ni, B Ratliff, et al. (2010) Renal capsule as a stem cell niche. American journal of physiology Renal physiology 298 (5): F1254-1262.
8. S Bruno, B Bussolati, C Grange, F Collino, LV di Cantogno, et al. (2009) Isolation and characterization of resident mesenchymal stem cells in human glomeruli. Stem cells and development 18 (6): 867-880.
9. I Shaw, S Rider, J Mullins, J Hughes, B Péault (2018) Pericytes in the renal vasculature: roles in health and disease. Nature Reviews Nephrology 14 (18): 521-534.

10. S Tanaka, D Portilla, MD Okusa (2023) Role of perivascular cells in kidney homeostasis, inflammation, repair and fibrosis. Nature reviews Nephrology 19 (11): 721-732.

11. S Aggarwal, A Moggio, B Bussolati (2013) Concise review: stem/progenitor cells for renal tissue repair: current knowledge and perspectives. Stem cells translational medicine 2(12): 1011-1019.

12. Q Liu, G Liu, D Sun, S Li (2026) Pretreated mesenchymal stromal cells and their secretome for kidney disease: mechanisms and applications. Stem cell research & therapy 17(1): 140.

13. Y Huang, P Chen, CB Zhang, GJ Ko, M Ruiz, et al. (2010) Kidney-derived mesenchymal stromal cells modulate dendritic cell function to suppress alloimmune responses and delay allograft rejection. Transplantation 90 (12): 1307-1311.

14. T Machiguchi, T Nakamura (2019) Nephron generation in kidney cortices through injection of pretreated mesenchymal stem cell-differentiated tubular epithelial cells. Biochemical and biophysical research communications 518 (1): 141-147.

15. FC Chang, YH Chou, YT Chen, SL Lin (2012) Novel insights into pericyte-myofibroblast transition and therapeutic targets in renal fibrosis. Journal of the Formosan Medical Association = Taiwan yi zhi 111 (11): 589-598.

16. ZH Liu, SY Li, BJ Li, F Zhang, XG Li, et al. (2025) Deciphering the Therapeutic Mechanisms of Wuzi Yanzong Pill for Asthenozoospermia: A Synergistic Approach Combining Bioinformatics and Molecular Dynamics. Cell biochemistry and biophysics 83 (4): 5181-5196.

17. T Pan, Q Xiao, HJ Fan, L Xu, SC Qin, et al. (2023) Wuzi Yanzong Pill relieves MPTP-induced motor dysfunction and neuron loss by inhibiting NLRP3 inflammasome-mediated neuroinflammation. Metabolic brain disease 38 (7): 2211-2222.

18. Y-r Li, H-j Fan, R-r Sun, L Jia, L-y Yang, et al. (2023) Wuzi Yanzong Pill Plays A Neuroprotective Role in Parkinson's Disease Mice via Regulating Unfolded Protein Response Mediated by Endoplasmic Reticulum Stress. Chinese Journal of Integrative Medicine 29 (1) :19-27.

19. Xiuhua Zhang, Shili Cao (2018) Current Status of Traditional Chinese Medicine in the Prevention and Treatment of Focal Segmental Glomerulosclerosis. Chinese Traditional and Herbal Drugs 49(1): 4688-4693.

20. Yifei Xu, Xiaoqian Yan, Enrui Zhang, Y Lu (2023) Clinical Experience of Professor LU Ying in the Treatment of Focal Segmental Glomerulosclerosis with Traditional Chinese Medicine. Chinese Journal of Integrated Traditional and Western Nephrology 24(1): 855-857.

21. Y Shi, X Shi, M Zhao, Y Zhang, Q Zhang, et al. (2023) Ferroptosis is involved in focal segmental glomerulosclerosis in rats, Scientific reports. 13 (1): 22250.

22. WQ Chen, CF Ding, J Yu, CY Wang, LY Wan, et al. (2020) Wuzi Yanzong Pill-Based on Network Pharmacology and *In Vivo* Evidence-Protects Against Spermatogenesis Disorder *via* the Regulation of the Apoptosis Pathway. Frontiers in pharmacology 11: 592827.

23. Y Zhu, T Tchkonia, T Pirtskhalava, AC Gower, H Ding, et al. (2015) The Achilles' heel of senescent cells: from transcriptome to senolytic drugs. Aging cell 14 (14): 644-658.

24. L J Hickson, L G P Langhi Prata, S A Bobart, T K Evans, N Giorgadze, et al. (2019) Senolytics decrease senescent cells in humans: Preliminary report from a clinical trial of Dasatinib plus Quercetin in individuals with diabetic kidney disease, EBioMedicine 47: 446-456.

25. M Lesjak, I Beara, N Simin, D Pintać, T Majkić, et al. (2018) Antioxidant and anti-inflammatory activities of quercetin and its derivatives, Journal of Functional Foods 40: 68-75.

26. Mahzari, S Li, X Zhou, D Li, S Fouda, et al. (2019) Matrine Protects Against MCD-Induced Development of NASH via Upregulating HSP72 and Downregulating mTOR in a Manner Distinctive from Metformin, Frontiers in pharmacology 10: 405.

27. M R Wang, X J Zhang, H C Liu, W D Ma, M L Zhang, et al. (2019) Matrine protects oligodendrocytes by inhibiting their apoptosis and enhancing mitochondrial autophagy, Brain research bulletin 153: 30-38.

28. L Yuan, J Yang, Y Li, L Yuan, F Liu, et al. (2022) Matrine alleviates cisplatin-induced acute kidney injury by inhibiting mitochondrial dysfunction and inflammation via SIRT3/OPA1 pathway, Journal of cellular and molecular medicine 26(13): 3702-3715.

29. F Wu, S Li, N Zhang, W Huang, X Li, et al. (2018) Hispidulin alleviates high-glucose-induced podocyte injury by regulating protective autophagy, Biomedicine & pharmacotherapy = Biomedecine & pharmacotherapie 104: 307-314.

30. D Julia Arró Díaz, O Naylan Castelnaux, A Ochoa Pacheco, Y Nascimento (2021) Antioxidant activity of bioactive compounds isolated from leaves and bark of Gymnanthes lucida Sw 33: 22-39.

31. Z Chen, Y Zou, H Sun, Y He, K Ye, et al. (2024) Engineered Enucleated Mesenchymal Stem Cells Regulating Immune Microenvironment and Promoting Wound Healing, Advanced materials (Deerfield Beach, Fla.) 36(45): 2412253.

32. J Pajarinen, T Lin, E Gibon, Y Kohno, M Maruyama, et al. (2019) Mesenchymal stem cell-macrophage crosstalk and bone healing. Biomaterials 196: 80-89.

33. Y Song, Y You, X Xu, J Lu, X Huang, et al. (2023) Adipose-Derived Mesenchymal Stem Cell-Derived Exosomes Biopotentiated Extracellular Matrix Hydrogels Accelerate Diabetic Wound Healing and Skin Regeneration. Advanced science (Weinheim, Baden-Wurttemberg, Germany) 10(30): 2304023.

34. M Belingheri, L Lazzari, V Parazzi, E Groppali, E Biagi, et al. (2013) Allogeneic mesenchymal stem cell infusion for the stabilization of focal segmental glomerulosclerosis. Biologicals: journal of the International Association of Biological Standardization 41(6): 439-445.

35. J Liang, J Zhao, L Yang, Q Wang, J Liao, et al. (2025) MSC-exosomes pretreated by Danshensu extracts pretreating to target the hsa-miR-27a-5p and STAT3-SHANK2 to enhanced antifibrotic therapy. Stem cell research & therapy 16(1): 40.

36. H Ma, Y Wu, Y Xu, L Sun, X Zhang (2013) Human umbilical mesenchymal stem cells attenuate the progression of focal segmental glomerulosclerosis. The American journal of the medical sciences 346(6): 486-493.

37. Q D Hu, R Z Tan, Y X Zou, J C Li, J M Fan, et al. (2023) Synergism of calycosin and bone marrow-derived mesenchymal stem cells to combat podocyte apoptosis to alleviate adriamycin-induced focal segmental glomerulosclerosis. World journal of stem cells 15 (6): 617-631.

38. X Ling, X Wang, J Li, T Zhang, X Zhou, et al. (2021) Shu-Di-Huang, Gan-Cao Herb Pair Restored the Differentiation Potentials of Mesenchymal Stem Progenitors in Treating Osteoporosis via Downregulation of NF-κB Signaling Pathway, Evidence-based complementary and alternative medicine: eCAM 7795527.

39. R Kramann, R K Schneider, D P DiRocco, F Machado, S Fleig, et al. (2015) Perivascular Gli1+ progenitors are key contributors to injury-induced organ fibrosis, Cell stem cell 16(1): 51-66.